structural characterization of CO-inhibited forms of CpI, as well as that of CpII and other Fe-only and NiFe hydrogenases, may contribute additional insights to the mechanistic details of reversible hydrogen oxidation catalyzed by the hydrogenase enzymes.

References and Notes

1. A. E. Pryzbyla, J. Robbins, N. Menon, H. D. Peck, *FEMS Microbiol. Rev.* **88**, 109 (1992).
2. M. W. W. Adams, *Biochim. Biophys. Acta* **1020**, 115 (1990).
3. R. K. Thauer, A. R. Klein, G. C. Hartmann, *Chem. Rev.* **96**, 3031 (1996).
4. A. Volbeda *et al.*, *Nature* **373**, 580 (1995).
5. J. C. Fontecilla-Camps, *J. Biol. Inorg. Chem.* **1**, 91 (1996).
6. A. Volbeda *et al.*, *J. Am. Chem. Soc.* **118**, 12989 (1996).
7. M. W. W. Adams, E. Eccleston, J. B. Howard, *Proc. Natl. Acad. Sci. U.S.A.* **86**, 4932 (1989).
8. A. T. Kowal, M. W. W. Adams, M. K. Johnson, *J. Biol. Chem.* **264**, 4342 (1989).
9. W. A. Hendrickson, *Science* **254**, 51 (1991).
10. CpI was purified from *C. pasteurianum* as described [J.-S. Chen and L. E. Mortenson, *Biochim. Biophys. Acta* **371**, 283 (1974)] with hydrogen evolution activity of 3400 μmol min^{-1} mg^{-1}. Crystallization was accomplished using the microcapillary batch diffusion method [M. M. Georgiadis, *Science* **257**, 1653 (1992)] and a precipitating solution of 25% polyethylene glycol 4000, 0.1 M sodium acetate (pH 4.6), and 0.2 M ammonium sulfate. The precipitating solution was allowed to slowly equilibrate with the protein solution [50 mM tris (pH 8.0) and 0.2 M KCl], resulting in a crystallization solution at an approximate pH of 5.1, which is near the pH optimum for hydrogen evolution activity of CpI at pH 5.0 [V. M. Fernández, *Anal. Biochem.* **130**, 54 (1983)]. Because of the oxygen sensitivity of CpI, sodium dithionite was used as a reductant to remove trace amounts of oxygen in both the precipitating solution and the protein samples. All manipulations were conducted in a vacuum atmospheres anaerobic chamber under an atmosphere of 100% N_2 at room temperature.
11. B. W. Matthews, *J. Mol. Biol.* **33**, 491 (1968).
12. For data collection, the crystals were equilibrated in a mother liquor solution (containing a final concentration of ~10% glycerol) and cooled to near liquid N_2 temperatures. Data for MAD phasing were collected at Stanford Synchrotron Radiation Laboratory (SSRL) beam line 1-5 equipped with a Hamlin charge-coupled device detector. The individual images were indexed using REFIX [W. Kabsch, *J. Appl. Crystallogr.* **24**, 795 (1993)], and the data were processed with MOSFLM [A. G. W. Leslie, *CCP4 and ESF-EACMB Newsletter on Protein Crystallography* (1992), p. 26] and scaled with SCALA of the CCP4 suite of crystallography software [Collaborative Computational Project No. 4, *Acta Crystallogr.* **D50**, 760 (1994)]. The 1.8 Å resolution data used in the final refinement were collected with Cu-K α radiation using a Rigaku RU300 x-ray generator equipped with a RAXIS-IIc phosphorimaging plate detector. The data were processed with DENZO and scaled with SCALEPACK [Z. Otwinowski, in *Data Collection and Processing*, L. Sawyer, N. Isaacs, S. Bailey, Eds. (CCP4 Study Weekend, SERC Daresbury Laboratory, Warrington, UK, 1991), pp. 56–62].
13. Initial Fe-S cluster sites could be identified using the program SOLVE [T. C. Terwilliger, *Acta Crystallogr.* **D50**, 17 (1994)], but even upon solvent flattening by SOLOMON [J. P. Abrahams and A. G. W. Leslie, *ibid.* **D52**, 30 (1996)] they were not interpretable with respect to the positions of individual amino acids; however, upon solvent flattening, the protein envelope was clearly visible. High-resolution phasing was obtained by assignment of the positions of the individual Fe atoms based on the limited degrees of freedom with respect to several of the clusters of known composition and the apparent sites of interaction between the protein and these clusters in the initial electron density maps (J. W. Peters and H. Bellamy, in preparation). When 16 Fe atoms were assigned with a reasonably high degree of certainty and were refined against the anomalous data, phasing could be extended to the full resolution of the MAD data (2.5 Å) and high-quality electron density maps were obtained upon solvent flattening. The high-quality initial electron density maps (calculated to 3.0 Å resolution) allowed all amino acid residues (574) of the sequence (*15*) and metal atoms to be placed with a high degree of certainty using the program O [T. A. Jones, J. Y. Zhou, S. W. Cowan, M. Kjeldgaard, *Acta Crystallogr.* **A47**, 110 (1991)]. Several rounds of positional and *B*-factor refinement [A. T. Brünger, J. Kuriyan, M. Karplus, *Science* **235**, 258 (1987)] of this initial model against the 1.8 Å resolution native data resulted in an R_{cryst} of 0.274 and an R_{free} of 0.313. This model was improved by iterative manual model building against $2F_{obs} - F_{calc}$ electron density maps and subsequent refinement. The present model exhibits good geometry, with 100% of the amino acid residues located in either most favorable or additionally allowed regions of the Ramachandran plot, as calculated with PROCHECK [R. A. Laskowski, M. W. McArthur, M. W. Moss, J. M. Thornton, *J. Appl. Crystallogr.* **26**, 283 (1993)]. The program PROMOTIF was used for secondary structure assignments [E. G. Hutchinson and J. M. Thornton, *Protein Sci.* **5**, 212 (1996)].
14. M. F. Gorwa, C. Croux, P. Soucaille, *J. Bacteriol.* **178**, 2668 (1996); S. Malki *et al.*, *ibid.* **177**, 2628 (1995); J. D. Santangelo, P. Durre, D. R. Woods, *Microbiology* **141**, 171 (1995); J. Stokkermans, W. van Dohngen, A. Kaan, W. van den Berg, C. Veeger, *FEMS Microbiol. Lett.* **58**, 217 (1989); G. Voordouw and S. Brenner, *Eur. J. Biochem.* **148**, 515 (1985); G. Voordouw, J. D. Strang, F. R. Wilson, *J. Bacteriol.* **171**, 3881 (1989).
15. J. Meyer and J. Gagnon, *Biochemistry* **30**, 9697 (1991).
16. R. H. Holm, P. Kennepohl, E. I. Solomon, *Chem. Rev.* **96**, 2239 (1996).
17. F. A. Cotton and G. Wilkinson, *Advanced Inorganic Chemistry* (Wiley, New York, 1988).
18. V. E. Kaasjager *et al.*, *Angew. Chem. Int. Ed.* **37**, 1668 (1998).
19. R. P. Happe, W. Roseboom, A. J. Pierik, S. P. J. Albracht, *Nature* **385**, 126 (1997).
20. T. M. Van Der Spek, *Eur. J. Biochem.* **237**, 629 (1996).
21. B. R. Crane, L. M. Siegel, E. D. Getzoff, *Science* **270**, 59 (1995).
22. H. Beinhart, R. H. Holm, E. Münck, *ibid.* **277**, 653 (1997).
23. J. Xia, Z. Hu, C. V. Popescu, P. A. Lindahl, E. Münck, *J. Am. Chem. Soc.* **119**, 8301 (1997).
24. K. A. Macor, R. S. Czernuszewicz, M. W. W. Adams, T. G. Spiro, *J. Biol. Chem.* **262**, 9945 (1987).
25. W. Fu *et al.*, *Biochemistry* **32**, 4813 (1993).
26. Brookhaven Protein Data Bank accession codes for the [2Fe-2S] ferredoxin from *Chlorella fusca* and the 2-[4Fe-4S] ferredoxin from *Chromatium vinosum* are 1awd and 1blu, respectively.
27. J. M. Moulis, L. C. Seiker, K. S. Wilson, Z. Dauter, *Protein Sci.* **5**, 1765 (1996).
28. H. Thomann, M. Bernardo, M. W. W. Adams, *J. Am. Chem. Soc.* **113**, 7044 (1991).
29. P. J. Stephens, D. R. Jollie, A. Warshel, *Chem. Rev.* **96**, 2491 (1996).
30. M. W. W. Adams, *J. Biol. Chem.* **262**, 15054 (1987).
31. _____, L. E. Mortenson, J.-S. Chen, *Biochim. Biophys. Acta* **594**, 105 (1980).
32. R. K. Thauer, B. Käufer, M. Zähringer, K. Jungermann, *Eur. J. Biochem.* **42**, 447 (1974).
33. W. I. Weis, R. Kahn, K. Drickamer, W. A. Hendrickson, *Science* **254**, 1608 (1991).

34. We thank H. Bellamy of SSRL for assistance in MAD data collection; F. Whitby and C. Hill of the University of Utah for use of their data collection facility for collection of preliminary data; and L. Berreau, S. Ensign, R. Holz, and J. Hubbard for helpful discussions. All figures were produced using MOLSCRIPT [P. J. Kraulis, *J. Appl. Crystallogr.* **24**, 946 (1991)] and RASTER3D [D. Bacon and W. F. Anderson, *J. Mol. Graphics* **6**, 219 (1988); E. A. Merritt and M. E. P. Murphy, *Acta Crystallogr.* **D50**, 869 (1994)]. Supported by NSF grants MCB-9807821 (J.W.P.) and MCB-9722937 (L.C.S.) and American Chemical Society–Petroleum Research Fund grant 33183-G4 (J.W.P.). The data collection facility at SSRL is funded by the U.S. Department of Energy, Office of Basic Energy Sciences, and by the NIH Biomedical Research Technology Program, Division of Research Resources. Coordinates have been deposited in the Brookhaven Protein Data Bank (accession code 1feh).

25 September 1998; accepted 30 October 1998

A 25,000-Year Tropical Climate History from Bolivian Ice Cores

L. G. Thompson, M. E. Davis, E. Mosley-Thompson, T. A. Sowers, K. A. Henderson, V. S. Zagorodnov, P.-N. Lin, V. N. Mikhalenko, R. K. Campen, J. F. Bolzan, J. Cole-Dai, B. Francou

Ice cores that were recovered from the summit of Sajama mountain in Bolivia provide carbon-14–dated tropical records and extend to the Late Glacial Stage (LGS). Oxygen isotopic ratios of the ice decreased 5.4 per mil between the early Holocene and the Last Glacial Maximum, which is consistent with values from other ice cores. The abrupt onset and termination of a Younger Dryas–type event suggest atmospheric processes as the probable drivers. Regional accumulation increased during the LGS, during deglaciation, and over the past 3000 years, which is concurrent with higher water levels in regional paleolakes. Unlike polar cores, Sajama glacial ice contains eight times less dust than the Holocene ice, which reflects wetter conditions and extensive snow cover.

A knowledge of tropical sensitivity to global paleoclimate changes and the abruptness of past changes is essential for modeling how the Earth's climate system responds during glacial stages and for simulating future climatic scenarios under warmer conditions that are anticipated from enhanced greenhouse gas concentrations (*1*). Recent research suggests that tropical proxy records may be more representative of global mean annual temperatures than proxy records from higher latitudes (*2*).

Several paleoclimatic records have been obtained from tropical glaciers, including a 1500-year history from the Quelccaya ice cap [13°56′S, 70°50′W, at 5670 m above sea level (asl)] in southern Peru (*3*) and a 20,000-year history from the col of Huascarán mountain (9°07′S, 77°37′W, at 6048 m asl) in the north central Peruvian Andes (*4*). We present an ice core record from Bolivia that provides a high-resolution tropical paleoclimate history of the Last Glacial Maximum (LGM), deglaciation, and the Holocene. The Sajama ice cap (18°06′S, 68°53′W, at 6542 m asl) covers the summit of an extinct volcano that sits on the northern boundary of what is currently a desert in the Altiplano (Fig. 1). The Altiplano has an average elevation of 3700 m and is the world's second largest plateau, covering about 205,000 km^2 (*5*). It is subdivided into a northern basin that is occupied by Lake Titicaca and a southern basin that consists of shallow saline lakes and salt flats, including the world's largest salt flat, the Salar de Uyuni (~12,500 km^2). On the southern Altiplano, the scant precipitation quickly evaporates, leaving salt crusts, except in part of the Poopó Basin, which is filled with a shallow hypersaline lake (Fig. 1) that is fed by the Rio Desaguadero with spillover drainage from Lake Titicaca (*6*).

Ice thicknsses on Sajama, determined with a short-pulse radar system, range from 121 to 177 m on the southeast flank of the volcano. A satellite-linked weather station installed at 6500 m asl in October 1996 records meteorological data (*7*). In 1997, four ice cores, two to bedrock [cores 1 (C-1) and 2 (C-2), at depths of 132.4 and 132.8 m, respectively] and two shallow cores (at depths of 40 and 4 m), were recovered with solar-powered electromechanical drills. The deep boreholes were separated by 3 m. Borehole temperatures ranged from –10.3°C at 10 m to –11.3°C between 30 and 70 m then warmed to –9.5°C at the ice-bedrock contact. The low temperatures throughout the ice cap ensured the preservation of a climatic and environmental record, and the basal temperature indicated that the ice was frozen to the bedrock. To accommodate gas analyses, we maintained the temperatures of the cores below –5°C without using dry ice from the time of drilling until analysis. C-1, the older record, was cut into 5063 continuous samples, which were analyzed for oxygen isotopic ratios of ice ($\delta^{18}O_{ice}$) and insoluble particulate (dust) and major anion (Cl^-, NO_3^-, and SO_4^{2-}) concentrations. Selected intervals were examined for ^{14}C-datable material, and

L. G. Thompson, M. E. Davis, K. A. Henderson, V. S. Zagorodnov, J. F. Bolzan, Byrd Polar Research Center, Department of Geological Sciences, The Ohio State University, Columbus, OH 43210, USA. E. Mosley-Thompson, Byrd Polar Research Center, Department of Geography, The Ohio State University, Columbus, OH 43210, USA. T. A. Sowers and R. K. Campen, Geosciences Department, Pennsylvania State University, University Park, PA 16802, USA. P.-N. Lin and J. Cole-Dai, Byrd Polar Research Center, The Ohio State University, Columbus, OH 43210, USA. V. N. Mikhalenko, Institute of Geography, Russian Academy of Sciences, Staromonetny 29, Moscow, 109017, Russia. B. Francou, ORSTOM, Apartado Postal 17 12 857, Quito, Ecuador.

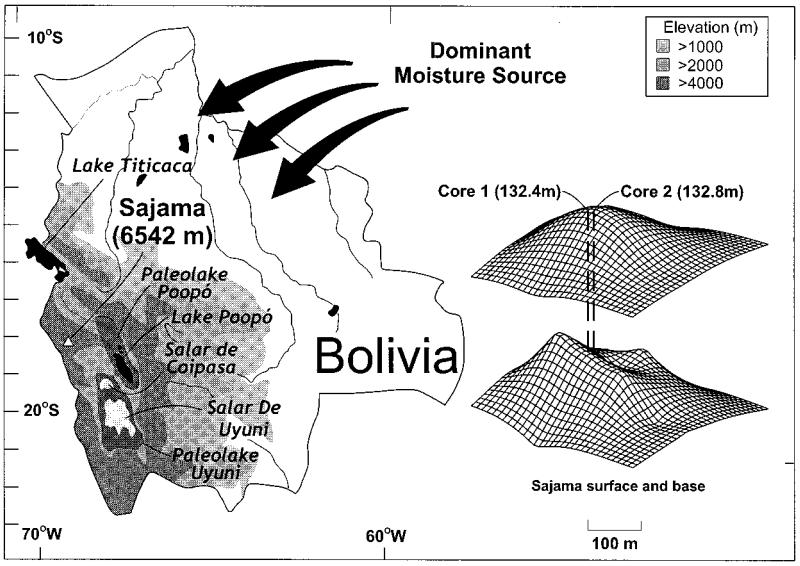

Fig. 1. Location of the Sajama ice cap in Bolivia (left) in relation to modern lakes (black) and salt flats (white). The dark gray areas were covered by paleolakes during the LGS. A schematic (right) depicts ice thicknesses on the summit and the locations of C-1 and C-2.

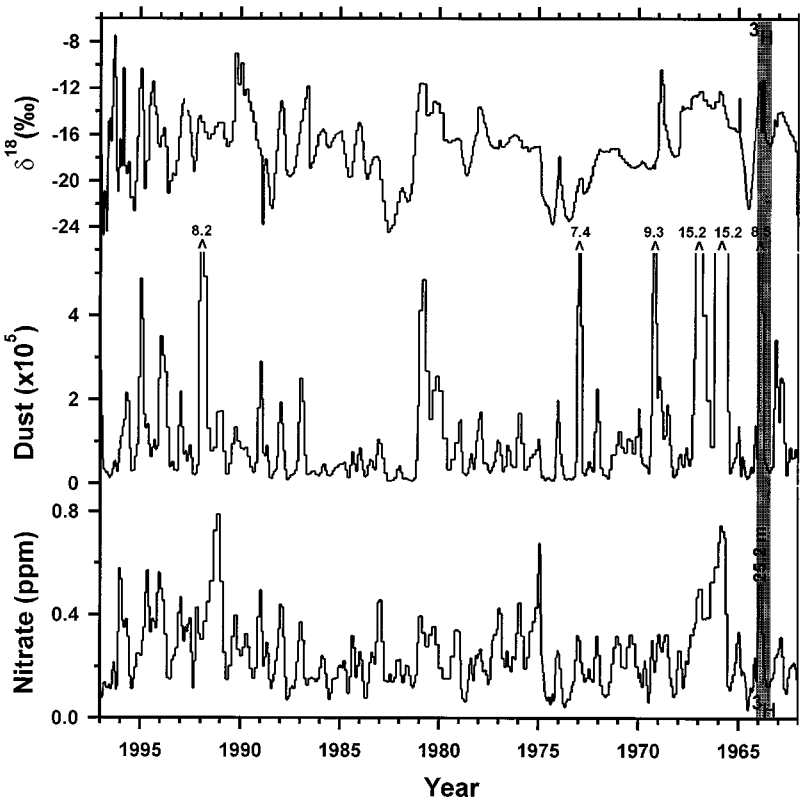

Fig. 2. Seasonal variations in $\delta^{18}O_{ice}$ (‰, per mil), insoluble dust, and NO_3^- concentrations (ppm, parts per million) allow layer counting in the upper part of C-1. Dating is calibrated by the identification of the 1964 ^3H peak (gray bars). The sample values in each plot are smoothed with a three-point (1, 2, 1) filter. Data are plotted so that annual tick marks correspond to the austral winter.

analyzed for gas composition and tritium (^{3}H). To demonstrate the reproducibility and continuity of the C-1 record, C-2 was also continuously analyzed for $\delta^{18}O_{ice}$, but at a lower resolution with fewer (803) samples.

The record. $\delta^{18}O_{ice}$, dust, and NO_3^- records in the upper part of C-1 show annual resolution, with the 1964 ^{3}H peak at 25.2 m (Fig. 2). The net accumulation was the equivalent of ~440 mm of H_2O over the uppermost 33 years, which is higher than the annual average of 316 mm in Sajama village (4220 m asl) at the base of the volcano (*8*).

The dust, $\delta^{18}O_{ice}$ values, and chemical species (Fig. 3) exhibit the greatest variations in the lowest 27 m of the cores. The $\delta^{18}O_{ice}$ values range from –20.7 per mil at the bottom of the core to –22.1 per mil between 125 and 115 m, where average dust concentrations are the lowest in the entire record. Low anion concentrations are interrupted between 124.5 and 120 m, where Cl^- increases sharply (centered on 123.8 m), SO_4^{2-} rises modestly, and NO_3^- declines. Small spikes in SO_4^{2-} and dust amounts occur near the peak of this chloride event.

From 114.5 to 110.5 m, $\delta^{18}O_{ice}$ values, dust, and anions increase abruptly. At 110.5 m, all ice core parameters abruptly decrease and remain low until 105.5 m, where $\delta^{18}O_{ice}$ values rapidly increase and remain high throughout the rest of the core. The dust content of the upper 103 m is much greater than in the lower 30 m; numerous dust layers are composed of large dark particles.

Time scale. The Sajama ice cores contain intact insects, insect fragments, and polylepis bark fragments with a sufficient mass for ^{14}C dating (Table 1). An abundance of plant material at 130.8 m in C-1 was split into two samples and independently dated by two accelerator mass spectrometry (AMS) facilities. The corrected ^{14}C dates (*9*) are 24,950 ± 430 years before the present (yr B.P.) (Lawrence Livermore National Laboratory) and 24,020 ± 140 yr B.P. (Woods Hole Oceanographic Institution), which confirm that Sajama contains LGM ice.

Between 11.5 and 20 kiloannum (ka) (105 and 130 m), an insufficient amount of ^{14}C-datable material was available for reliable AMS dating. Additional stratigraphic information for this section of the core was obtained by measuring the $^{18}O/^{16}O$ ratio of paleoatmospheric O_2 ($\delta^{18}O_{atm}$) trapped in the bubbles. We measured $\delta^{18}O_{atm}$ (*10, 11*) in 31 discrete samples between 56 and 130 m and compared our results with those from the Greenland Ice Sheet Project (GISP) 2 core (Fig. 4) (*12*). Although the Sajama $\delta^{18}O_{atm}$ record agrees with the GISP 2 record in some places (between 9 and 13 ka and between 16 and 24 ka), some Sajama data points do not fall within ±0.05 per mil of the corresponding GISP 2 data. The majority of these anomalous samples contain elevated $\delta Ar/N_2$ values (*13*) that are higher than any ice core sample measured to date (*14*).

To develop an age model for C-1, we used the ^{3}H-calibrated annual layer counts of the most recent 100 years (Fig. 2) and 10 samples that were isolated for radiocarbon dating (Fig. 3). The ^{14}C dates were converted into calendar ages (Table 1) with the latest calibration curves (*9, 15*). One ash horizon (Huaynaputina, A.D. 1600) was identified (*16*), and two depths were assigned ages by corre-

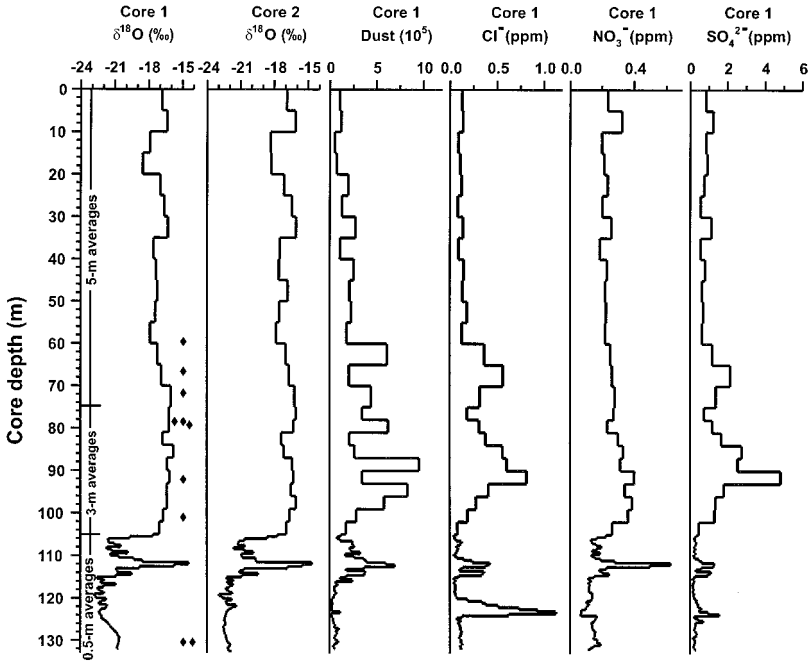

Fig. 3. Depth profiles of $\delta^{18}O_{ice}$ for C-1; $\delta^{18}O_{ice}$ for C-2; and concentrations of dust, Cl^-, NO_3^-, and SO_4^{2-} for C-1. Dust concentrations are the number of insoluble particles with diameters of ≥0.63 and ≤16.0 μm per milliliter of sample, and anion concentrations are in ppm. Locations of ^{14}C samples in the core are denoted by diamonds.

Table 1. Time-stratigraphic markers used in the development of the Sajama time scale are listed. The ^{14}C dates were converted to calendar years (yr B.P.) with a revised calibration procedure [method A (*15*)] using the bidecadal tree ring data set and a 24-year subtraction for the Southern Hemisphere. AMS ages for the two samples at a depth of 130.8 m were calibrated with the polynomial formula (*9*) based on ^{14}C- and U/Th-dated corals. $\delta^{18}O_{atm}$ dates were obtained in a manner similar to that described in (*12*). The age of the ice from these depths was determined by initially dating the gases through the correlation with the GISP 2 $\delta^{18}O$. We used a densification model (*52*) to calculate the differences (ice age – gas age) for these two samples assuming that the accumulation rate was 0.4 m/year and temperature was –12°C. The resulting difference was 65 years.

Depth (m)	Carbon (mg)	Dating technique	^{14}C dates (yr B.P.)	$^{14}C_{cal}$ ages with [1σ range] or (calendar age, yr B.P.)
25.2	NA	^{3}H	NA	−14 (A.D. 1964)
41.5	NA	Layer counts	NA	53 (A.D. 1897)
59.3	0.31	^{14}C AMS plant*	210 ± 70	150 [0–296]†
64.8	NA	Huaynaputina	NA	350 ± 0
67.0	0.37	^{14}C AMS plant*	380 ± 50	354 [311–485]
72.1	0.08	^{14}C AMS plant‡	1,460 ± 290	1,310 [1058–1681]
78.1	0.11	^{14}C AMS plant‡	2,350 ± 230	2,340 [2047–2732]
78.3	0.09	^{14}C AMS plant*	920 ± 130	780 [671–936]§
78.3	0.10	^{14}C AMS plant*	1,250 ± 120	1,160 [980–1282]§
92.1	0.42	^{14}C AMS plant*	3,220 ± 70	3,390 [3353–3469]
100.6	0.15	^{14}C AMS insect‡	4,910 ± 180	5,610 [5334–5882]
101.2	NA	GISP 2 $\delta^{18}O_{atm}$	NA	9,100 ± 500
103.8	NA	GISP 2 $\delta^{18}O_{atm}$	NA	10,300 ± 600
130.8	0.43	^{14}C AMS wood‖	20,400 ± 120	24,020 [23,880–24,160]
130.8	0.13	^{14}C AMS wood*	21,200 ± 370	24,950 [24,520–25,380]

*Lawrence Livermore (nondiluted samples). †Indistinguishable from modern period, within a 1σ range. ‡Woods Hole (diluted samples), excluded from time scale construction because a potential problem with the dilution technique was unresolved at the time of paper submission. §The average of these two dates was used. ‖Woods Hole National Ocean Sciences AMS facility (nondiluted sample).

lating the $\delta^{18}O_{atm}$ data from Sajama with the GISP 2 $\delta^{18}O_{atm}$ record dated by layer counting (*17*). For the Holocene, an empirically derived depth-age function (Fig. 5) was generated (*18*) from seven definitive horizons or matching points (Table 1); this function was used to produce the time series profile of Sajama $\delta^{18}O_{atm}$ (Fig. 4). A clear change in the depth-age relationship occurs at 103.8 m (Fig. 5) and signifies an apparent increase in the average accumulation rate. Between 103.8 and 130.8 m, there are no stratigraphic markers to constrain the dating. The $\delta^{18}O_{atm}$ results below 115 m confirm the existence of LGM ice, but they cannot be used for dating because the $\delta^{18}O_{atm}$ values between 14 and 24 ka are uniform (1.0 per mil) (Fig. 4).

For dating the glacial portion of the Sajama record, matching respective records of $\delta^{18}O_{atm}$ and $\delta^{18}O_{ice}$ from Sajama and GISP 2 (*18*) produced similar results (Fig. 4). The bottom age of the core (~25.0 ka) is fixed by the reproducible ^{14}C dates at 130.8 m (1.5 m above the bed). The similarity of the major and minor $\delta^{18}O_{ice}$ events in Sajama and GISP 2 (assuming temporal synchroneity) allows the identification of 14 matching points between 104 and 123 m (Fig. 5). The $\delta^{18}O_{ice}$ record is also similar to the Huascarán $\delta^{18}O_{ice}$ record, which was dated by comparison with a ^{14}C-dated deep-sea foraminifera record of $\delta^{18}O_{CaCO_3}$ (*4, 19*). The differences in the resolution of the glacial portions of the Sajama and Huascarán records result from the different thicknesses of the LGS sequences—3 m in the Huascarán core versus 28 m in the Sajama core.

Establishing dated horizons in C-1 enables us to estimate an accumulation history. The observed depth-age profile suggests that annual layers thin much more rapidly in the upper part of the ice cap than predicted by simple laminar flow or by numerical modeling of ice divide deformation (*20*). The observed thinning is similar to that seen in ice caps at Dunde, China (*21*), and Guliya, China (*22*). In the absence of the appropriate data (*23*), we assume that the vertical velocity profile is similar to that inferred from the Dunde and Guliya ice cores. If changes in ice thickness are ignored, the average accumulation rate a_{ij} between the dated depth horizons z_i and z_j (where i, and j, are any two dated horizons) is given by

$$a_{ij} = \frac{1}{\Delta t_{ij}} \int_{z_i}^{z_j} \left(1 - \frac{z}{H}\right)^{-p} dz \qquad (1)$$

where H is the ice thickness, z is the ice-equivalent depth, p is a constant, and Δt_{ij} is the number of years between z_i and z_j.

On the basis of results from the Dunde and Guliya ice caps, we reconstructed accumulation rate histories for $p = 1.5$ and 2. Although the reconstructed accumulation rates vary greatly as a function of p, both reconstructions produce similar trends (the average is shown in Fig. 6). The regional accumulation rate was relatively high between ~25 and 16 ka and reached a minimum at ~14 ka. Between 14 and ~11.5 ka, the accumulation rate increased and then decreased between 11.5 and 3 ka. It has increased from 3 ka to the present.

The LGS and deglaciation. The synchronous changes in anion concentrations are unlikely to have resulted from changes in regional source strength or from changes in transport efficiency. The anions have different sources, as NO_3^- is predominantly terrestrial in origin and SO_4^{2-} and Cl^- are most often ascribed to marine sources. In the LGM, Cl^- concentrations increased, whereas NO_3^- concentrations decreased; at 14 ka, all

Table 2. Comparison of the averages of $\delta^{18}O_{ice}$ for the modern period (0 to 1 ka), the early Holocene (EH) (6.8 to 10 ka), and the LGM (18 to 21.2 ka) and the differences between them for the cores shown in Fig. 7. The averages of two time intervals for the LGM are given for the Vostok core to account for the ~3000-year lead time (*12*). The $\delta^{18}O$ equivalents ($\delta D = 8\delta^{18}O + 10$) are shown in parentheses.

Core sites	Modern	EH	LGM	LGM-modern (per mil)	LGM-EH (per mil)
Sajama (Bolivia)	−16.8	−16.7	−22.1	5.4	5.4
Huascarán (Peru)	−18.5	−16.6	−22.9	4.4	6.3
GISP 2 (Greenland)	−35.0	−34.6	−39.7	4.7	5.1
Guliya (Western China)	−14.4	−13.1	−18.5	4.1	5.4
Byrd (Antarctica)	−32.8	−33.9	−40.5	7.6	6.6
Vostok* (Antarctica)	−441 (−56.4)	−436 (−55.7)	−472 (−60.2)	3.9	4.5
Vostok† (Antarctica)	−441 (−56.4)	−436 (−55.7)	−479 (−61.1)	4.8	5.4

*Interval, 18 to 21.2 ka. †Interval, 21 to 24.2 ka.

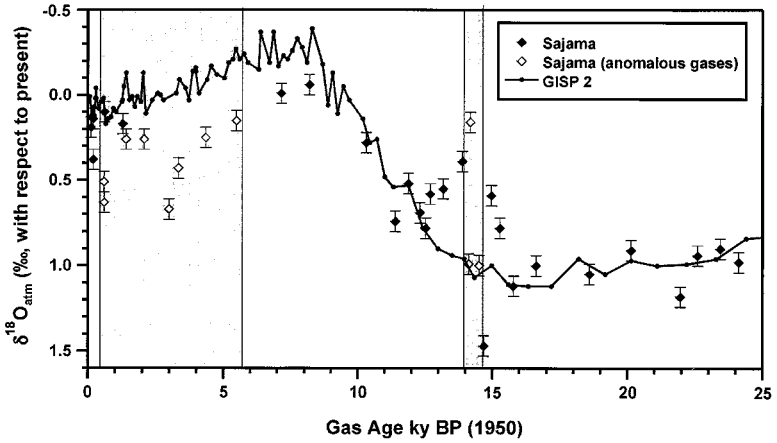

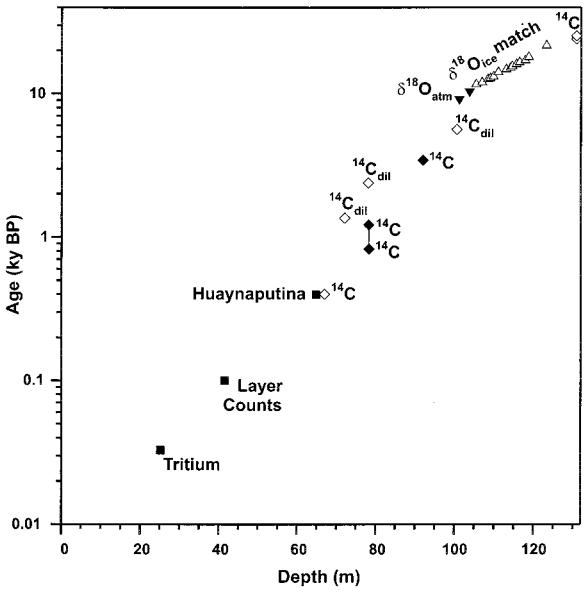

Fig. 4 (left). $\delta^{18}O_{atm}$ values from GISP 2 (*12*) are compared to the Sajama $\delta^{18}O_{atm}$ record. The shaded areas denote Sajama data points that lie outside ±0.05 per mil of the corresponding GISP 2 data and contain elevated $\delta Ar/N_2$ values. **Fig. 5 (right).** All data used to constrain the Sajama time scale are illustrated to show the depth-age relationship. Diamonds denote ^{14}C data, triangles denote $\delta^{18}O_{ice}$ matching points, and squares signify absolute dates. Solid symbols represent the data points used to construct the Holocene time scale (*18*). The dates from the ^{14}C data points at 78.3 m were averaged (denoted by the line between them) because of their low individual carbon weights (Table 1).

anion species increased simultaneously. Moisture on Huascarán and Sajama originates from the east, over the Amazon River basin (*4, 8*). However, the 14-ka anion concentration event on Sajama (located on the Altiplano) is absent in the Huascarán ice core to the north of the Altiplano. A comparison of the LGM anion event is not possible because the Huascarán record is <20 ka. Therefore, changes in anion concentrations on Sajama appear to have been heavily influenced by local changes in source strength. It is likely that increases in anion concentrations, particularly in SO_4^{2-} and in Cl^-, are tied to the desiccation of the Altiplano lakes; when the lakes are dry, salts containing SO_4^{2-} and Cl^- are entrained by winds over the salt flats and then deposited in snow on the ice cap.

One-hundred-year averages of the 25,000-year (25-ky) Sajama record (Fig. 6) provide a high-resolution view of the LGS (11.5 to 25 ka). Layers of large dark particles, derived from the flanks of Sajama and neighboring volcanoes, are absent in this core section because the regional snowline was 800 to 900 m lower during the LGM (*24*). Remote sensing studies (*25*) in the central Andes (5° to 23°S) show that the present snow line rises from east to west because precipitation decreases with increasing distance from the moisture sources, which are the tropical Atlantic and the Amazon River basin. The snow line during the LGM likely varied in a similar manner.

At times during the LGS, much of the Altiplano was covered by large paleolakes (*26–28*); these have been mostly dry throughout the Holocene, when large salt flats such as the Salar de Uyuni were exposed. Cold, wet conditions on the Altiplano from 25 to 22 ka are indicated in the Sajama record by depleted $\delta^{18}O_{ice}$ values, low anion concentrations, and a high regional precipitation of dust (Fig. 6). This period is believed to coincide with the latter phase of Minchin Lake, which covered an area between ~40,000 and 60,000 km^2 or more (*26*). The large increase in Cl^- (and, to a lesser extent, SO_4^{2-}) and a large decrease in net accumulation at ~22 ka indicate that these lakes began to dry and reached a maximum desiccation at ~21 ka, after which the lakes slowly refilled (~2000 years).

Aerosol concentrations suggest that the lake basins retained water until 15.5 ka, when warm, dry conditions abruptly ensued. Contained in 4 m of core, this progressive and oscillating warming (culminating at ~14.3 ka) is the isotopically warmest (–14 per mil) interval in the 25-ky record. The aridity of this warm period is evident from increases in dust and all three major anions, suggesting that the drying of the lakes on the Altiplano was more regional and was different from the drying that occurred during the latter part of the LGS, when only SO_4^{2-} and Cl^- increased.

After the interstadial, a deglaciation climatic reversal (DCR) began at 14 ka as the climate shifted abruptly to colder conditions that were similar to those attributed to the North Atlantic Younger Dryas (YD) stadial. The Sajama DCR is characterized by a

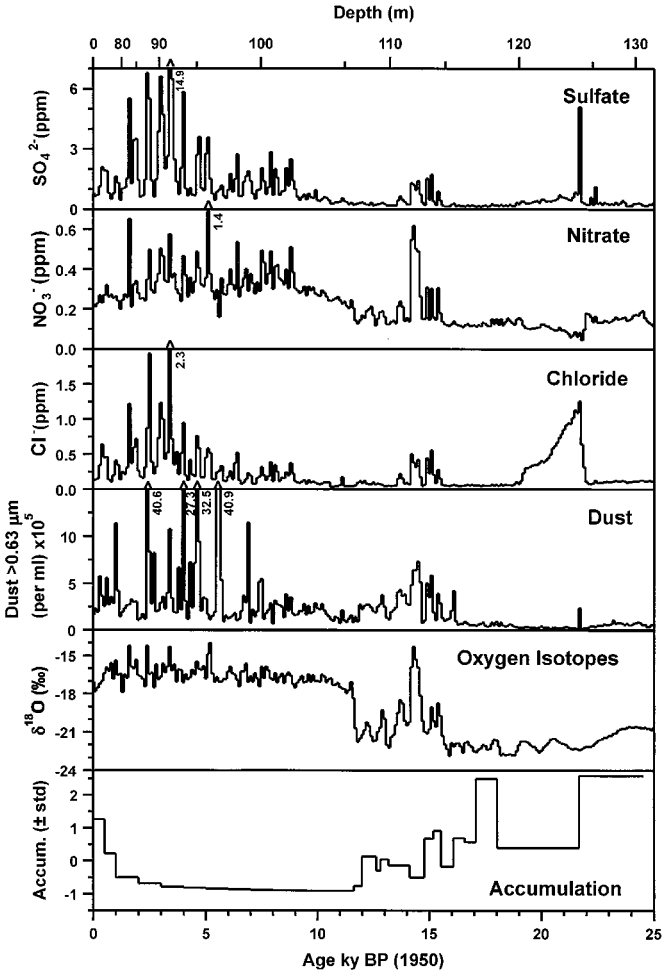

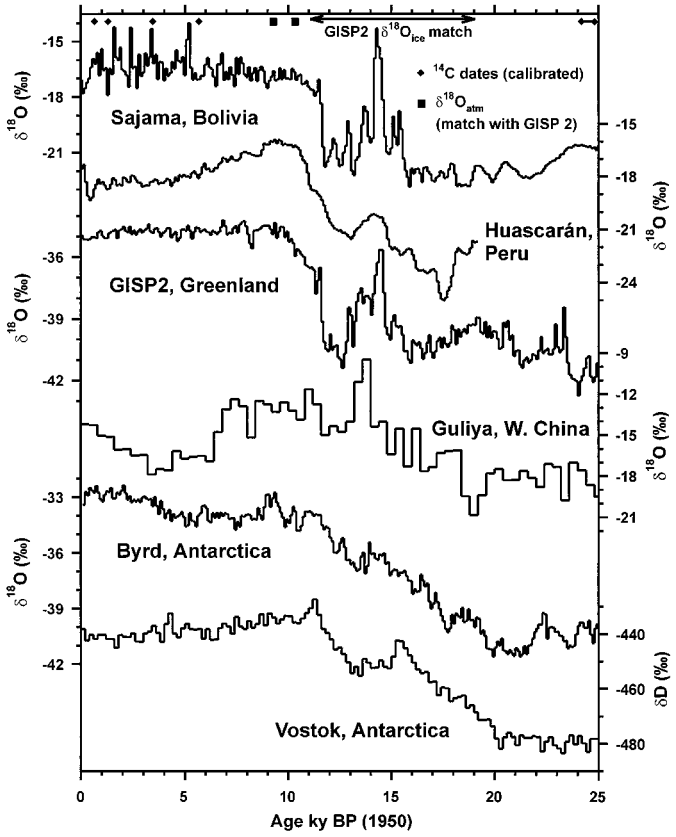

Fig. 6 (left). The 100-year averages of $\delta^{18}O_{ice}$; insoluble dust; and Cl^-, NO_3^-, and SO_4^{2-} concentrations from C-1 are shown for the past 25,000 years. Dating is based on ^{14}C dates and on matching $\delta^{18}O_{atm}$ and $\delta^{18}O_{ice}$ with GISP 2. Two accumulation histories (p = 1.5 and 2.0) were calculated with Eq. 1. The two accumulation records were combined (averaged), and the data presented are deviations from the mean of the combined record. **Fig. 7 (right).** The global extent of the LGS and a climatic reversal (cooling) during deglaciation is illustrated by the stable isotope records from two tropical sites [Sajama and Huascarán (*4*)], two Northern Hemisphere sites [Guliya (*22*) and GISP 2 (*29*)], and two Southern Hemisphere sites [Byrd station (*47*) and Vostok (*48*)]. All records shown are 100-year averages, except records for Vostok (200-year averages) and Guliya (400-year averages). δD, $8\delta^{18}O + 10$.

$\delta^{18}O_{ice}$ decrease from the previous interstadial, comparable to that in the Greenland (*29*) ice cores (5.2 versus 5.3 per mil). As in the LGM, the cold climate during the DCR on Sajama was accompanied by higher net accumulation (Fig. 6) and high lake stands as inferred from decreases in aerosol concentrations. Palynologic and glacial geological studies elsewhere in the Andes (*27, 30*) confirm that the initial rise of Tauca Lake did not result from melting glaciers but from a precipitation increase over the Altiplano. However, lake desiccation at the termination of the DCR was more gradual and continued well into the Holocene.

Dust concentrations in ice cores from both Sajama and Huascarán show a slight decrease in dust loading during the DCR, which is consistent with dust concentrations in Antarctic cores (*31*) but in contrast to the dustiness of the YD in the Greenland ice core records (*32*). These differences suggest that dust loading associated with the YD may have been restricted to the Northern Hemisphere as the possible product of the glacial flour generated along the fluctuating margins of the large Northern Hemisphere ice sheets.

The Holocene. The colder conditions of the DCR persisted until 11.5 ka, when a sudden warming occurred within a few centuries, marking the onset of the Holocene (Fig 6). At 105 m, $\delta^{18}O_{ice}$ values increased from an average of –20.5 to –16.5 per mil (Fig. 3), after which they increased only slightly to the tops of the ice cores. Soluble and insoluble aerosol concentrations remained low until ~9 ka, when abrupt increases in deposition signaled a drop in lake levels. The insoluble dust concentration in the Holocene is eight times that in the LGM, which is inconsistent with dust records from polar ice cores (*31, 32*). The enhanced dust concentration is a result not only of increased local volcanic activity but also of the elevated Holocene snowlines and of decreased net accumulation (Fig. 6) that occurred at the beginning of the Holocene and continued until ~3.4 ka. The high concentrations of soluble species and dust indicate that the lake levels were low in the mid-Holocene from 9 ka (lagging the accumulation decrease by ~2.5 ky) to 3 ka on the Altiplano. Water levels in Lake Titicaca in the northern basin were also low from ~7.7 to 3.5 ka (^{14}C dating) (*33*). The subsequent decrease in aerosols from ~3 ka to the present reflects an increasing accumulation in the region (Fig. 6), which is consistent with slightly higher levels in Lake Titicaca (*34*).

Climatic implications. The paleoclimate record preserved in the Sajama ice cores strongly reflects the waxing and waning of the paleolakes, a dominant feature of the Altiplano (*35*). The presence or absence of these lakes reflects regional changes in the climate system. On the Altiplano, cold periods were generally wet, unlike the conditions inferred from polar ice cores. Glaciers in the cordilleras of southern Peru and Bolivia appear to have expanded before the last global glacial maximum (*36*), implying that cooler global temperatures were associated with greater precipitation and reduced evaporation in the subtropical Andes. Such changes would result from more frequent incursions of polar air masses from the southeast, as they bring cooler and cloudier conditions to the subtropical Andes throughout much of the year (*37*). However, under current conditions, >80% of the annual precipitation at the base of Sajama falls within the summer months (November through March) and is associated with increased solar radiation. This heating of the Altiplano enhances convection, which facilitates moist air advection from the east (*8*).

The similarity of the $\delta^{18}O_{ice}$ values from Huascarán (Peru) and Sajama (Table 2) suggests that the Amazon River basin has remained the dominant moisture source for the tropical Andes. The drier conditions on Huascarán at 9°S (*4*) and the wetter conditions on Sajama at 18°S during the LGS are consistent with lake-level reconstructions for that time period (*38*), when only 25% of the tropical lakes that have been studied had levels that were as high as present levels. In the Northern Hemisphere, lake levels increased poleward, so that, between 25° and 35°N, most of the lake levels were higher than present levels (*39*). Model experiments (*1*) indicate that this difference is consistent with a reduction in both the tropical latitudinal temperature gradient and Hadley cell intensity. These results require that the tropical Atlantic was ~5°C cooler at the LGM (*40*), which is a greater cooling than inferred from the CLIMAP (Climate: Long-Range Investigation, Mapping, and Prediction) (*41*) simulation. A reduced temperature gradient at low to subtropical latitudes weakens the Hadley circulation regardless of the mean temperature, which plays a secondary role (*42*). These interpretations are consistent with other LGM precipitation reconstructions (*43*). The enhanced moisture content of LGM and DCR air masses and prolonged cloud cover would contribute to substantial increases in accumulation and to reduced evaporation.

The question of whether the YD affected the Southern Hemisphere remains controversial (*4, 44, 45*). Results from Taylor Dome, Antarctica (*45*), show a cold reversal that was contemporaneous with the YD in Greenland. The Sajama record confirms the existence of a DCR at 18°S on the Altiplano of Bolivia, which is consistent with the Huascarán record from 9°S. The interstadial at ~14.7 ka is more pronounced on Sajama and on the Guliya ice cap (*22*) than it is in polar cores (Fig. 7). Similarly, the magnitude of the subsequent rapid cooling is greater on Sajama, suggesting that the DCR was an important climate event in the tropics. This pronounced event, which extends 4.5 m (or 2500 years) on Sajama, exhibits a rapid onset and termination, which occur in less than a few centuries. Both the DCR and the YD in Greenland are characterized by a 5.2 per mil decrease in mean $\delta^{18}O_{ice}$ from Holocene values. The near synchroneity of changes in methane source regions and the temperature response at the end of the YD in Greenland supports an atmospheric transmission of the climate signal (*46*). The abrupt onset and termination of the DCR suggest that atmospheric processes are also likely to have driven the climate changes associated with it. These data have implications for the role of the tropical hydrological system as a key driver of abrupt global climate changes (*46*).

The time scale for the Sajama cores allows a comparison of their $\delta^{18}O_{ice}$ profiles (Fig. 7) with other tropical (*4*), subtropical (*21, 22*), and polar records (*29, 47, 48*). This global array of cores shows large-scale similarities and important regional differences. From the early Holocene (6.8 to 10.0 ka) to the LGM (18.0 to 21.2 ka), $\delta^{18}O_{ice}$ values shift by 5.1 per mil in the GISP2 core (*29*), 6.3 per mil in the Huascarán core (*4*), and 6.6 per mil in the Byrd core (*47, 49*). All of these cores show similar isotopic depletion (Table 2), as do the differences between modern (0 to 1000 yr B.P.) and LGM values. This depletion reflects substantial global cooling in the LGM, which is consistent with records from other archives [such as snow line depression, noble gases from groundwater in the Amazon River basin, and corals (*50*)], although these data suggest a greater cooling than recent foraminiferal and alkenone reconstructions (*51*).

References and Notes

1. D. Rind, *J. Geophys. Res.* **103**, 5943 (1998).
2. R. S. Bradley, *NATO ASI Ser. Ser. I* **41**, 603 (1996).
3. L. G. Thompson, E. Mosley-Thompson, J. F. Bolzan, B. R. Koci, *Science* **229**, 971 (1985).
4. L. G. Thompson *et al.*, *ibid.* **269**, 46 (1995).
5. A. Kessler, *Erdkunde* **22**, 275 (1963).
6. C. M. Clapperton, J. D. Clayton, D. I. Benn, C. J. Marden, J. Argollo, *Quat. Int.* **38/39**, 49 (1997).
7. D. R. Hardy, M. Vuille, C. Braun, F. Keimig, R. S. Bradley, *Bull. Am. Meteorol. Soc.* **79**, 1899 (1998).
8. M. Vuille, D. R. Hardy, C. Braun, F. Keimig, R. S. Bradley, *J. Geophys. Res.* **103**, 11191 (1998).
9. E. Bard, *Geochim. Cosmochim. Acta* **62**, 2025 (1998).
10. To a first approximation, the $\delta^{18}O_{atm}$ record follows the $\delta^{18}O$ of seawater over the past 135 ka [T. Sowers *et al.*, *Paleoceanography* **8**, 737 (1993); (*11, 12*)]. Because the turnover time of atmospheric O_2 (~1500 years) is much longer than the interhemispheric mixing (~1 year), records of $\delta^{18}O_{atm}$ must be the same for all ice cores that accurately record the composition of the atmosphere. As such, $\delta^{18}O_{atm}$ has been used to place ice core climate records from Greenland and Antarctica on a common time scale for investigating interhemispheric climate connections (*11, 12*).
11. M. T. Bender *et al.*, *Nature* **372**, 663 (1994)
12. T. Sowers and M. Bender, *Science* **269**, 210 (1995).
13. $\delta Ar/N_2 = 1000 \times [(^{40}Ar/^{14}N_2)_{sample}/(^{40}Ar/^{14}N_2)_{standard}] - 1$.

14. Because the Ar/N_2 ratio of the atmosphere must have remained constant for the past 10^6 years [T. Sowers, M. L. Bender, D. Raynaud, *J. Geophys. Res.* **94**, 5137 (1989)], any deviations in the $\delta Ar/N_2$ values (after correcting for gravitational fractionation) indicate that additional factors have altered the composition of the trapped air parcels. Of the 31 samples measured for gas composition, 8 had elevated $\delta Ar/N_2$ values (maximum $\delta Ar/N_2 = 80$ per mil), whereas all 31 samples had $\delta O_2/N_2$ values that were similar to those found in polar cores ($\delta O_2/N_2$ between 2.0 and −48.7 per mil) [M. T. Bender, T. Sowers, V. Lipenkov, *J. Geophys. Res.* **100**, 18651 (1995)]. One possible explanation for these data involves a local O_2-depleted air source (such as soil gas) in contact with surface melt features (potentially on the grain boundaries) that are subsequently incorporated into the ice matrix in the firn-ice transition region below.
15. M. Stuvier and P. J. Reimer, *Radiocarbon* **35**, 215 (1993).
16. The location of the Huaynaputina ash in C-1 (64.85 m) was confirmed by nearby ^{14}C dates at 59 and 67 m and by the comparison of its chemistry with that from a bulk Huaynaputina ash sample of the A.D. 1600 eruption collected at the Cerro Trapiche archeological site in Peru. Both samples were analyzed for major elements on an Optima 3000 inductively coupled plasma–optical emission spectrometer (ICP-OES) (Perkin-Elmer, Norwalk, CT). The analytical results (in percent) are as follows (Cerro Trapiche ash, Sajama ash): SiO_2 (70.09, 71.00), Al_2O_3 (14.41, 14.74), Na_2O (3.93, 3.87), K_2O (2.76, 3.36), FeO (3.22, 3.00), CaO (3.58, 2.15), TiO_2 (0.53, 0.53), and MgO (1.48; 1.35).
17. R. B. Alley *et al.*, *J. Geophys. Res.* **102**, 26367 (1997).
18. This function [age $= 10 \exp(-2.42 + 0.045z - 3.85 \times 10^{-4}z^2 + 2.62 \times 10^{-6}z^3)$, where z = depth below surface] provides a monotonic depth-age model for the Holocene that circumvents abrupt layer thickness changes across individual matching points that would result from a stepwise model (that is, assuming a constant layer thickness between dated horizons). Slight deviations from the individual ascribed dates occur in the model, although the departure of the modeled age scale from the seven horizons is <10% of each individual age. For glacial-stage ice (before 9.7 ka), the AnalySeries 1.0a program [D. Paillard, L. Labeyrie, P. Yiou, *Eos* **77**, 379 (1996)] was used to transfer the depth-based Sajama geochemical records to the GISP 2–based time scale. Constant layer thicknesses were used between the 14 $\delta^{18}O_{ice}$ matching points, because large abrupt shifts were no longer a concern as little layer thinning is apparent in the glacial-stage ice.
19. E. Bard *et al.*, *Nature* **328**, 791 (1987).
20. C. R. Raymond, *J. Glaciol.* **29**, 357 (1983).
21. L. G. Thompson *et al.*, *Science* **246**, 474 (1989).
22. L. G. Thompson *et al.*, *ibid.* **276**, 1821 (1997).
23. To reconstruct a more exact accumulation history, one needs the vertical strain rate, which is the fractional change in layer thickness per unit time, as a function of depth. This quantity is very difficult to measure directly and usually must be inferred from surface velocity measurements and modeling results. Here, no velocity measurements were made, and in the absence of other physical data, detailed ice-flow modeling is not possible.
24. D. Rind and D. Peteet, *Quat. Res.* **24**, 1 (1985).
25. A. G. Klein, B. L. Isacks, A. L. Bloom, *Bull. Inst. Fr. Etud. Andines* **24**, 607 (1995).
26. C. M. Clapperton, *Quaternary Geology and Geomorphology of South America* (Elsevier, Amsterdam, 1993), p. 498.
27. G. O. Seltzer, *Boreas* **23**, 105 (1994).
28. M. Servant and J. C. Fontes, *Cah. ORSTOM Ser. Geol.* **14**, 15 (1978).
29. P. M. Grootes, M. Stuvier, J. W. C. White, S. Johnsen, J. Jouzel, *Nature* **366**, 552 (1993).
30. G. O. Seltzer, *J. Quat. Sci.* **7**, 87 (1992).
31. L. G. Thompson and E. Mosley-Thompson, *Science* **212**, 812 (1981).
32. C. U. Hammer *et al.*, in *Greenland Ice Core: Geophysics, Geochemistry, and the Environment*, vol. 33 of *Geophysical Monograph Series*, C. C. Langway Jr., H. Oeschger, W. Dansgaard, Eds. (American Geophysical Union, Washington, DC, 1985), pp. 77–84; K. C. Taylor *et al.*, *Nature* **361**, 432 (1993).
33. D. Wirrman, P. Mourguiart, L. F. de Oliveira Almeida, in *Quaternary of South America and Antarctic Peninsula,* J. Rabassa, Ed. (Balkema, Rotterdam, 1988), vol. 6, pp. 89–129; D. Wirrman and P. Mourguiart, *Quat. Res.* **43**, 344 (1995).
34. M. B. Abbott, M. W. Binford, M. Brenner, K. R. Kelts, *Quat. Res.* **47**, 169 (1997).
35. J. Minchin, *Proc. R. Geogr. Soc.* **4**, 67 (1882).
36. C. M. Clapperton, *Palaeogeogr. Palaeoclimatol. Palaeoecol.* **101**, 189 (1993).
37. G. O. Seltzer, *Quat. Sci. Rev.* **9**, 137 (1990).
38. F. A. Street-Perrott and S. P. Harrison, in *Climate Processes and Climate Sensitivity,* vol. 29 of *Geophysical Monograph Series*, J. E. Hansen and T. Takahashi, Eds. (American Geophysical Union, Washington, DC, 1984), pp. 118–129.
39. W. S. Broecker, D. Peteet, I. Hajdas, J. Lin, E. Clark, *Quat. Res.* **50**, 12 (1998); L. V. Benson, *ibid.* **16**, 390 (1981); L. V. Benson, *J. Paleolimnol.* **5**, 115 (1991).
40. R. S. Webb, D. H. Rind, S. J. Lehman, R. J. Healy, D. Sigman, *Nature* **385**, 695 (1997); A. Ganopolski, S. Rahmstorf, V. Petoukhov, M. Claussen, *ibid.* **391**, 351 (1998).
41. CLIMAP Project Members, *Science* **191**, 1131 (1976); CLIMAP, *Geol. Soc. Am. Map Chart Ser. MC-36* (1981).
42. D. Rind, personal communication.
43. T. J. Crowley and S. T. Baum, *J. Geophys. Res.* **102**, 16463 (1997).
44. V. Markgraf, *Boreas* **20**, 63 (1991); A. C. Ashworth and V. Markgraf, *Rev. Chil. Hist. Nat.* **62**, 61 (1989); K. A. Hughen *et al.*, *Nature* **391**, 65 (1998); T. V. Lowell *et al.*, *Science* **269**, 1541 (1995).
45. E. J. Steig *et al.*, *Science* **282**, 92 (1998).
46. J. P. Severinghaus, T. Sowers, E. J. Brook, R. B. Alley, M. L. Bender, *Nature* **391**, 141 (1998).
47. S. J. Johnsen, W. Dansgaard, H. B. Clausen, C. C. Langway Jr., *Nature* **235**, 429 (1972).
48. J. Jouzel *et al.*, *ibid.* **329**, 403 (1987).
49. The isotopic shift in the Byrd core is probably amplified by ice originating from higher, colder locations during the glacial stage [W. F. Budd and N. W. Young, in *The Climatic Record in Polar Ice Sheets*, G. de Q. Robin, Ed. (Cambridge Univ. Press, Cambridge, 1983), pp. 167–168].
50. S. C. Porter, *Geol. Soc. Am. Bull.* **90**, 980 (1979); D. G. Herd and C. W. Naeser, *Geology* **2**, 603 (1974); H. A. Osmaston, thesis, Oxford University (1965); W. S. Broecker and G. H. Denton, *Quat. Sci. Rev.* **9**, 305 (1990); M. Stute *et al.*, *Science* **269,** 379 (1995); T. P. Guilderson, R. G. Fairbanks, J. L. Rubenstone, *ibid.* **263**, 663 (1994).
51. E. Bard, F. Rostek, C. Sonzogni , *Nature* **385**, 707 (1997); T. Wolff, S. Mulitza, H. Arz, J. Pätzold, G. Wefer, *Geology* **26**, 675 (1998).
52. M. M. Herron and C. C. Langway Jr., *J. Glaciol.* **25**, 373 (1980).

53. We thank the many scientists, engineers, technicians, graduate students, and support personnel from The Ohio State University and ORSTOM; the people of Sajama village, Bolivia; U. Schotterer for ^3H analyses; J. Olesik for the ICP-OES results on the Huaynaputina ash; S. Lehman, J. Turnbull, J. Southon, A. McNichol, S. Handwork, D. Stuart, and J. Donoghue for the AMS dates; B. Pouyaud and J. Argollo for making this logistically challenging field program possible; the Polar Ice Coring Office for the use of a drill; and, particularly, B. Koci and the mountain guides of the Casa de Guias, Huaraz, Peru. This work was supported by NOAA and NSF. This is contribution 1110 of the Byrd Polar Research Center.

11 September 1998; accepted 2 November 1998